Naval Research Laboratory
Washington, DC 20375-5000

AD-A212 839

Numerical Evaluation of the Far Field Wave Pattern of the Radiation Green's Function

HENRY T. WANG* AND E. WADE MINER**

*Center for Fluid/Structure Interactions
**Center for Fluid/Dynamic Developments
Laboratory for Computational Physics and Fluid Dynamics

September 5, 1989

89 9 26 162

REPORT DOCUMENTATION PAGE

1a REPORT SECURITY CLASSIFICATION	1b RESTRICTIVE MARKINGS
UNCLASSIFIED	

2a SECURITY CLASSIFICATION AUTHORITY	3 DISTRIBUTION / AVAILABILITY OF REPORT
	Approved for public release; distribution unlimited.
2b DECLASSIFICATION / DOWNGRADING SCHEDULE	

4 PERFORMING ORGANIZATION REPORT NUMBER(S)	5 MONITORING ORGANIZATION REPORT NUMBER(S)
NRL Memorandum Report 6478	

6a NAME OF PERFORMING ORGANIZATION	6b OFFICE SYMBOL (If applicable)	7a NAME OF MONITORING ORGANIZATION
Naval Research Laboratory	Code 4420	

6c. ADDRESS (City, State, and ZIP Code)	7b ADDRESS (City, State, and ZIP Code)
Washington, DC 20375-5000	

8a. NAME OF FUNDING / SPONSORING ORGANIZATION	8b. OFFICE SYMBOL (If applicable)	9 PROCUREMENT INSTRUMENT IDENTIFICATION NUMBER
Office of Naval Research		

8c. ADDRESS (City, State, and ZIP Code)	10 SOURCE OF FUNDING NUMBERS			
	PROGRAM ELEMENT NO	PROJECT NO	TASK NO RR023-	WORK UNIT ACCESSION NO
Arlington, VA 22217	61153N		01-41	DN158-17

11 TITLE (Include Security Classification)

Numerical Evaluation of the Far Field Wave Pattern of the Radiation Green's Function

12. PERSONAL AUTHOR(S)

Wang, H.T. and Miner, E.W.

13a TYPE OF REPORT	13b TIME COVERED	14. DATE OF REPORT (Year, Month, Day)	15 PAGE COUNT
Interim	FROM 1/87 TO 10/88	1989 September 5	28

16 SUPPLEMENTARY NOTATION

17 COSATI CODES			18 SUBJECT TERMS (Continue on reverse if necessary and identify by block number)
FIELD	GROUP	SUB-GROUP	Far field wave pattern Translating oscillating source
			Radiation Green's function
			Computer program RADGREEN

19 ABSTRACT (Continue on reverse if necessary and identify by block number)

Computer program RADGREEN has been developed to calculate the far field wave pattern of the radiation Green's function corresponding to an oscillating source translating below the free surface. The program has the capability of calculating the Green's function and its derivatives, or the associated wave elevation and slopes. The far field analysis is based on an asymptotic formulation which neglects terms which are of order 1/R and higher. Techniques for removing and attenuating singularities in the formulation and eliminating short noise-like waves are described in some detail. A number of three-dimensional and contour plots are given to show sample radiation wave patterns for a single source and for a line of sources whose strengths are adjusted to approximate those for a ship hull undergoing heave or pitch motions.

20 DISTRIBUTION / AVAILABILITY OF ABSTRACT	21 ABSTRACT SECURITY CLASSIFICATION
☒ UNCLASSIFIED/UNLIMITED ☐ SAME AS RPT ☐ DTIC USERS	UNCLASSIFIED

22a NAME OF RESPONSIBLE INDIVIDUAL	22b TELEPHONE (Include Area Code)	22c OFFICE SYMBOL
Henry T. Wang	(202) 767-2516	Code 4420

DD Form 1473, JUN 86   Previous editions are obsolete   SECURITY CLASSIFICATION OF THIS PAGE

S/N 0102-LF-014-6603

CONTENTS

iii

NUMERICAL EVALUATION OF THE FAR FIELD WAVE PATTERN
OF THE RADIATION GREEN'S FUNCTION

1. INTRODUCTION

The method of Green's functions is widely used to analyze the flow around surface ship hulls. If one neglects very short waves, such that surface tension and viscosity effects may be neglected, these functions represent potentials of point sources which are chosen to satisfy all the required conditions of the problem with the exception of the kinematic condition of no flow through the ship hull. This latter condition, in turn is used to determine the strengths of the sources which are placed on the hull surface.

A critical step in this procedure is the efficient evaluation of the near field behavior of the Green's function to determine the mutual influence of the sources. Once these influences have been determined, the problem reduces to a system of simultaneous linear equations for the source strengths. The near field behavior is also of interest in obtaining the pressure distribution on the hull surface, as well as the bow wave in such applications as slamming and deck wetness.

The far field analysis is often used to obtain the damping and resistance forces due to the waves generated by the motions of the ship. This usually leads to a more accurate determination than the direct integration of the hull pressure distribution due to the greater simplicity and higher resolution of the far field analysis. More recently, with the advent of more accurate remote sensing techniques, the far field wave pattern is also of interest from the detection point of view.

The three most widely used Green's functions, listed in increasing order of complexity, are the ring wave (or zero speed) function for an oscillating stationary source, the Kelvin (or wave resistance) function for a nonoscillating translating source, and the general case of the radiation (or ship motions) function for an oscillating translating source. For the simple ring wave case, Liu [1] derived near and far field solutions as early as 1952. This simple case is characterized by the fact that there is exactly one wave at each field point and in the far field these waves form circular rings around the source. More recently, Grekas and Delhommeau [2] show that in the case of low speed the far field ring waves have elliptic shape. The far field wave pattern of the Kelvin source has been widely studied since this gives rise to wave resistance, the drag component which may be most significantly reduced by suitable ship design. It is well known that there are two waves (transverse and divergent) inside a triangular region behind the ship, with a half angle of 19.47°. The various far field approaches are summarized in the classical paper by Eggers, Sharma, and Ward [3]. It is only in recent years that Newman [4], and Wang and Rogers [5] have derived efficient computational schemes for the near field flow.

For the general radiation case, where the source is both oscillating and translating, efficient robust computational schemes for the near field flow appear to be lacking. A notable exception may be the work by Chang [6]. In the far field case, Newman [7] has outlined a computational approach for obtaining the wave pattern. This report presents a numerical implementation of this formulation. First, a brief description of the derivation of the far field expressions is given. Next, various aspects of carrying out their numerical evaluation are described in some detail. These include an efficient

1

iterative scheme for finding the wave propagation directions at a given field point, the treatment of singular points and lines in the formulation, a grid filtering technique to eliminate short waves which appear as noise, and an efficient method of extending the procedure for a single source to a line of sources which may be taken to represent the ship hull in the far field. Expressions are developed for the values of the Green's function and its slopes, as well as for the associated wave elevation and its slopes. Numerical results are presented in the form of computer generated three-dimensional and contour plots for various cases of a single source and a line of sources. These figures show in particular, the differences between the pattern of the Green's function and the wave elevation, between the functions (Green and elevation) and their slopes, and between the wave elevations due to a single source and a line of sources modeling heave (linear vertical oscillatory motion) and pitch (rotational oscillatory motion in the vertical centerplane). The report concludes with a summary of the calculation procedure and the numerical results.

2. DESCRIPTION OF FAR FIELD FORMULATION

For the sake of uniformity, the present report will consistently follow the coordinate system and notation used in [7]. This coordinate system is shown in Fig. 1, and corresponds to the source at rest in the presence of a current c in the $-x$ direction, which is equivalent to the source traveling at speed c in the $+x$ direction. The y axis corresponds to the horizontal direction perpendicular to x, and the z axis is directed vertically upwards.

2.1 Derivation of Far Field Formulas for Values of G_{11} for Single Source

Assume that the Green's function G is expressed in the form

$$G(x,y,z;\xi,\eta,\zeta;t) = \text{Re}\left\{G_{11}(x,y,z;\xi,\eta,\zeta)e^{i\omega t}\right\}$$

where x,y,z and ξ,η,ζ are respectively the coordinates of the field point and source shown in Fig. 1, t is time, and ω is the circular frequency of oscillation. In the above equation and in the remainder of this report, only the real part of the complex expression is of interest and, for the sake of convenience, the symbol Re will be omitted hereafter. G_{11} must satisfy the following conditions

$$\nabla^2 G_{11} = 0; \quad z < 0; \quad (x,y,z) \neq (\xi,\eta,\zeta) \tag{2a}$$

$$-\omega^2 G - 2i\omega c\, \frac{\partial G_{11}}{\partial x} + c^2\frac{\partial^2 G_{11}}{\partial x^2} + g\frac{\partial G_{11}}{\partial z} = 0 \tag{2b}$$

$$\lim_{z \to -\infty} \frac{\partial G_{11}}{\partial z} = 0 \tag{2c}$$

$$\lim_{R \to \infty} \nabla G = 0 \tag{2d}$$

In addition, a radiation condition of no incoming waves at $R \to \infty$ is needed to ensure uniqueness of the solution. Using the Fourier transform approach, G_{11} is given by

$$G_{11} = \frac{1}{r} - \frac{1}{r'} + F_1 + F_2 + F_3 \tag{3}$$

where $r = [(x - \xi)^2 + (y - \eta)^2 + (z - \zeta)^2]^{1/2}$, $r' = [(x - \xi)^2 + (y - \eta)^2 + (z + \zeta)^2]^{1/2}$, F_1, F_2, F_3 are double integrals of the complex wavenumber λ and the real wave propagation direction u.

The analysis is considerably simplified by neglecting terms which are of order $1/R$ or higher, where R is related to x and y by

$$R = (x^2 + y^2)^{1/2} \tag{4a}$$

$$x = R \cos \theta \tag{4b}$$

$$y = R \sin \theta \tag{4c}$$

$$\theta = \tan^{-1}(y/x) \tag{4d}$$

In the above, θ is the spatial direction. By using the calculus of residues and the method of stationary phase on the double integrals F_1, F_2, and F_3, the following algebraic expression for the far field values of G_{11} is obtained

$$G_{11}(R,\theta,z;\xi,\eta,\zeta) = \left[\frac{8\pi}{R}\right]^{1/2} \sum_u \text{sign}(\cos u) \left[\frac{\lambda_i \sin^2 \theta}{\sin^2 u \left|\frac{d\theta}{du} \cos (u - \theta)\right|}\right]^{1/2} \times$$

$$\exp\left\{\lambda_i(u)[z + \zeta + iR \cos (u - \theta) - i\xi \cos u - i\eta \sin u] + \frac{\pi i}{2} + \text{sign}\left[\frac{\partial^2 g_i}{\partial u^2}\right]\frac{\pi i}{4}\right\} \tag{5}$$

The wavenumber $\lambda_i(u)(i = 1,2)$ is given by

$$\lambda_i = \frac{\nu}{2\tau^2 \cos^2 u} [1 + 2\tau \cos u \pm (1 + 4\tau \cos u)^{1/2}] \tag{6}$$

where the upper sign is used for $i = 1$ and the lower sign for $i = 2$, $\tau = \omega c /g$, $\nu = \omega^2/g$, g is the gravity constant, and the function $g_i(u)$ is given by

$$g_i = \lambda_i \cos (u - \theta) \tag{7}$$

Equation (5) is to be summed over the values of u which give $\partial g_i /\partial u = 0$. This in turn gives rise to the following transcendental $u - \theta$ equation

$$\text{ctn} \ \theta = - \left[\tan u \pm \frac{(1 + 4\tau \cos u)}{\sin u \cos u}\right] \tag{8}$$

where u is in the interval $-\pi \leq u \leq \theta - \pi/2$, and again the upper and lower signs are to be used for $i = 1$ and 2, respectively. Fig. 2, which corresponds to Fig. 1 of Ref. [7], shows plots of the above equation for various values of the parameter τ. The diagonal line connecting the points $(\theta = 0, u = -\pi/2)$ and $(\theta = \tau, u = \pi/2)$ represents the upper limit of permissible values of u. This figure shows that there may be anywhere from zero to 5 roots, depending on θ and τ.

2.2 Limiting Cases of $\tau \to 0$.

Since the above formulation is for a translating oscillating source, it should contain in the limit of values of $\tau(=c\omega/g) \to 0$ the ring wave case for $c \to 0$ and the Kelvin wave case for $\omega \to 0$.

The ring wave case is recovered by taking the lower sign in Eq. (6), setting $\tau \cos u = \epsilon$, and expanding the square root term to second power in ϵ resulting in

$$\lambda_2 = \frac{\nu}{2\epsilon^2} \left\{ 1 + 2\epsilon - \left[1 + \frac{4\epsilon}{2} - \frac{(4\epsilon)^2}{8} \right] \right\} = \frac{\nu}{2\epsilon^2} 2\epsilon^2 = \nu \equiv \frac{\omega^2}{g} \qquad (9)$$

which is precisely the wavenumber of the zero speed case. The Kelvin waves may be recovered by taking the upper sign in Eq. (6), noting that $\nu/\tau^2 = \omega^2 g^2/c^2\omega^2 = g^2/c^2$ gives the fundamental wavenumber λ_c of the Kelvin waves, once again setting $\tau \cos u = \epsilon$, and expanding the square root term to first power in ϵ, resulting in

$$\lambda_1 = \frac{\lambda_c}{2 \cos^2 u} \left[1 + 2\epsilon + \left[1 + \frac{4\epsilon}{2} \right] \right] = \frac{\lambda_c(2 + 2\epsilon)}{2 \cos^2 u} \to \frac{\lambda_c}{\cos^2 u}, \epsilon \to 0 \qquad (10)$$

The term $\lambda_c/\cos^2 u$ gives the precise variation of the wavelengths of the Kelvin wake with wave propagation direction u.

2.3 Derivatives of the Green's Function

Often it is of interest to determine not only the values of the Green's function but also its x and y derivatives. In the case of damping force and remote detection applications, it is not the Green's function itself but the associated wave elevation and slopes which are of principal interest. All of these derivative quantities may be conveniently obtained from the formula for G_{11} given in Eq. (5).

Recalling that this equation is a far field expression for large values of R, the operations $\partial/\partial x = \partial/\partial(R \cos \theta)$ and $\partial/\partial y = \partial/\partial(R \sin \theta)$ would add a power of $1/R$ to most terms in Eq. (5). The only term for which this is not the case involves the exponential function

$$\left[\frac{\partial}{\partial x}, \frac{\partial}{\partial y} \right] \exp [\lambda_i iR \cos (u - \theta)] = \left[\frac{\partial}{\partial x}, \frac{\partial}{\partial y} \right] [\lambda_i i(x \cos u + y \sin u)] \qquad (11)$$

for which the derivatives $\partial/\partial x$ and $\partial/\partial y$ are equivalent to multiplying the function by $i\lambda_i \cos u$ and $i\lambda_i \sin u$, respectively. Thus, the x and y derivatives of G_{11} are simply given by

$$\frac{\partial G_{11}}{\partial x} = \left[\frac{8\pi}{R} \right]^{1/2} \sum i\lambda_i \cos u \ G_{11i} \qquad (12a)$$

4

$$\frac{\partial G_{11}}{\partial y} = \left[\frac{8\pi}{R}\right]^{1/2} \sum i\lambda_i \sin u \; G_{11i} \qquad (12b)$$

where G_{11i} refers to the entire expression after the summation sign in Eq. (5). The elevation z_s of the wave pattern for the present case of an oscillating source in the presence of a current c in the $-x$ direction, shown in Fig. 1, is given by

$$z_s = \frac{-1}{g}\left[\frac{\partial G_{11}}{\partial t} - c\,\frac{\partial G_{11}}{\partial x}\right] = \left[\frac{8\pi}{R}\right]^{1/2} \sum -\frac{i}{g}(\omega - c\lambda_i \cos u)G_{11i} \qquad (13)$$

The x and y slopes are then obtained similar to Eqs. (12)

$$\frac{\partial z_s}{\partial x} = \left[\frac{8\pi}{R}\right]^{1/2} \sum \frac{-i}{g} i\lambda_i \cos u (\omega - c\lambda_i \cos u)\, G_{11i} \qquad (14a)$$

$$\frac{\partial z_s}{\partial y} = \left[\frac{8\pi}{R}\right]^{1/2} \sum \frac{-i}{g} i\lambda_i \sin u (\omega - c\lambda_i \cos u)\, G_{11i} \qquad (14b)$$

2.4 Extension to Multiple Sources

The straightforward way of evaluating the Green's function for a series of N sources with strengths Q_j and locations (ξ_j, η_j, ζ_j) is to repeat the calculation of Eq. (5) N times and sum over the results. Actually, as a result of the far field assumptions inherent in Eq. (5), the computational effort for N sources differs very little from that for one source. Most of the computational effort in evaluating G_{11} occurs in the iterative search for the various u-roots of Eq. (8) for a given value of θ. Eq. (5) shows, however, that θ and R are always measured from the origin even though the source may be located at (ξ, η, ζ). This assumption is possible since $R >> (\xi, \eta, \zeta)$. Thus, only the exponential term $\exp\{\lambda_i(u)[\zeta - i\xi \cos u - i\eta \sin u]\}$ varies for the different sources. The term $\lambda_i \zeta$ gives the decrease in the strength of the source due to submergence ζ below the free surface while the term $-i\xi \cos u - i\eta \sin u$ gives the shift in the phase of the wave originating from (ξ, η) relative to the wave due to a source located at $(0,0)$.

A particularly useful configuration for modeling ship hulls in the far field is a line of N sources with the same values of η and ζ, but different values of Q_j and ξ_j. In this case, the value of G_{11} at a given field point (x, y, z) is given by the following double sum

$$G_{11} = \left[\frac{8\pi}{R}\right]^{1/2} \sum_u \text{sign}\,(\cos u)\left\{\frac{\lambda_i \sin^2 \theta}{\sin^2 u \;|\frac{d\theta}{du}\cos(u - \theta)|}\right\}^{1/2} \times$$

$$\exp\left\{\lambda_i[z + \zeta + iR\cos(u - \theta) - i\eta \sin u] + \frac{\pi i}{2} + \text{sign}\left[\frac{\partial^2 g_i}{\partial u^2}\right]\frac{\pi i}{4}\right\} \times$$

$$\sum_{j=1}^{N} \frac{Q_j}{4\pi i} \exp\left(-i\xi_j \cos u\right) \tag{15}$$

Similar expressions hold for extending the derivatives of G_{11}, the elevation z_s and its slopes for a single source, given in Eqs. (12) to (14), to a line of sources.

3. COMPUTER IMPLEMENTATION OF THEORETICAL FORMULATION

The preceding formulation has been numerically implemented in the form of the FORTRAN 77 computer program RADGREEN. The present chapter describes the more complex or novel aspects of the implementation. Input, output, and computer time requirements of the program are also described to give an indication of actual usage.

3.1 Iterative Solution for Wave Propagation Direction

The most time consuming part of the procedure is the finding of the zero to five values of u which correspond to a given value of θ in Eq. (8). The solution scheme essentially consists of a global search to bracket the root values of u within certain bounds, and then a localized search to pinpoint the precise values.

The global scheme is contained in subroutine FINROOT, which evaluates the error functions f_1 and f_2 (for given values of θ and τ) for 721 equally spaced values of u between -180 and 0 degrees. The error functions f_1 and f_2 are defined as the difference between the left and right sides of Eq. (8) using the upper $(\lambda_1$ case) and lower $(\lambda_2$ case) signs, respectively. Where the function changes sign between two adjacent values of u, indicating a zero crossing and hence the location of a root, these values of u are identified and saved as initial bounds for a more precise determination by subroutine FR1. This subroutine closes in on the value of the root by an interval halving technique where the error function is evaluated at the midpoint between the bounds, and then moving the bound with the same sign of the error function to the midpoint. This iterative procedure is continued until the error function has an absolute value less than 10^{-6}. The resulting value of u and the associated wavenumber case $(\lambda_1$ or λ_2) are then returned to the main program for use in Eq. (5).

3.2 Treatment of Singular Points and Lines

Perhaps the most obvious indication that Eq. (5) is for the far field is the factor $1/\sqrt{R}$, which $\to \infty$ as $R \to 0$. Where calculations are desired for field points relatively close to the origin, the program provides the option for the user to input a minimum bound on values of R to be used in Eq. (5). For the zero speed case, Liu [1] shows that the far field formulation becomes valid for $R \geq 0.3\, l_2$, where l_2 is the wavelength and is related to the wavenumber λ_2 given in Eq. (9) by

$$l_2 = \frac{2\pi}{\lambda_2} = \frac{2\pi g}{\omega^2} \tag{16}$$

Eq. (5) shows that the factor contained within brackets may be singular at values of θ where $\sin u = 0$, $\cos(u - \theta) = 0$, $d\theta/du = 0$, and (due to Eq. (6) for λ_i) $\cos u = 0$. Actually, the singularities due to $\sin u$ and $\cos u$ are completely removable while the behavior at $\cos(u - \theta) \to 0$ is also regular. Thus, only the case $d\theta/du = 0$ is an actual singularity in the calculation.

The removable nature of the singularities for sin u and cos u may best be illustrated by explicity writing out $d\theta/du$ obtained by differentiating Eq. (8) with respect to u, resulting in

$$\frac{d\theta}{du} = \frac{\sin^2 \theta}{\sin^2 u \cos^2 u}[\sin^2 u \pm (-2\tau \sin u) \sin u \cos u /\sqrt{1 + 4\tau \cos u}$$

$$\pm (-1)\sqrt{1 + 4\tau \cos u} \cos 2u]$$ (17)

It is seen that the factors $\sin^2 \theta/\sin^2 u$ and $1/\cos^2 u$ are cancelled by corresponding factors in Eqs. (5) and (6). Thus, Eq. (5) is entirely free of singularities in terms of possible zeroes of sin u and cos u.

The regular behavior at cos $(u - \theta) \to 0$ may be seen by noting that this implies (since $|u - \theta| = \pi/2$ or $3\pi/2$ in Eq. (8)) that

$$1 + 4\tau \cos u_t = 0$$ (18)

and, from Eq. (6), that $\lambda_1 = \lambda_2$. From Fig. 2, and also by considering Eq. (17), it is seen that at these values of u the slope $du/d\theta = 0$, so that the product $\cos(u - \theta)d\theta/du$ has the indeterminate behavior 0/0. Numerical calculations show that the product has finite values, with resultant values of the magnification factor μ decreasing from 7.0 for $\tau = 0.26$ to 0.5 for $\tau = 1.0$, where μ is given by

$$\mu = \frac{\sin^2 \theta}{\sin^2 u \left| \frac{d\theta}{du} \cos (u - \theta) \right|}$$ (19)

The calculations show that the values of μ vary relatively slowly with small changes in u away from u_t. Since the indeterminate behavior does not involve two factors which exactly cancel as in the previous cases of sin u and cos u, it is numerically necessary to give special treatment to this factor for u near u_t. This is implemented in the computer program by restricting u, for cases of $\tau > 0.25$ and $u < 0$, to be at least 0.1 deg greater than u_t, i.e. $u \geq u_t + 0.1$ deg. To obtain the correct limiting behavior, the values of θ corresponding to this revised value of u must be obtained from Eq. (8) and used in Eq. (5).

Figure 2 shows that for θ near 180 deg, there may be two values of θ, θ_c, at which there is a vertical tangent $d\theta/du = 0$. These are the so-called cusp lines which give rise to unbounded values of G_{11} and also serve as bounding lines such that the waves are contained within the angular region $\theta_c \leq \theta \leq 180$ deg. This singular behavior illustrates the limitations of the present method since actual values of G_{11} are finite at the cusp lines and also extend outside these lines. Higher order asymptotic methods, such as that of steepest descent, are currently under investigation to obtain more accurate calculations of G_{11} on and near the cusp lines.

A particularly simple and well known case is obtained by setting Eq. (17) equal to 0, with $\tau = 0$, and taking the upper sign (λ_1 case) resulting in the following equation for u_c

$$\tan^2 u_c = 1/2 \Rightarrow u_c = 35.16 \text{ deg}$$ (20)

By substituting this equation in Eq. (8) the corresponding value of θ_c is found to be

$$\theta_c = 180. - 19.47 = 160.53 \text{ deg} \qquad (21)$$

This, of course, refers to the well known Kelvin waves for a nonoscillating translating ship for which the transverse and divergent waves meet at the cusp line with propagation angle 35.16 deg and the waves are confined within an angle at 19.47° to the $-x$ axis. Since $u > 0$, these waves (located above the $u = 0$ axis in Fig. 2) are propagating against the current (i.e., with the ship) while the remaining waves (located below the $u = 0$ axis) are propagating with the current.

It is of interest to ascertain the manner of this singular behavior as $u \rightarrow u_c$ for $\tau = 0$. The close bunching of the different curves for the Kelvin like waves above the $u = 0$ axis suggests that this behavior may also be applicable for other values of τ. The analysis consists of evaluating the magnification factor μ for small increments Δu away from u_c, i.e., evaluating Eq (19) with $u = u_c + \Delta u$. Numerical evaluation of the subsequent expression shows that μ varies approximately as

$$\mu \approx 13.5 / \Delta u \qquad (22)$$

where Δu is expressed in degrees. For a number of reasons it is necessary to set an upper limit on μ. Besides possible numerical overflow problems, excessively large values near the cusp line would tend to overwhelm the values elsewhere so that they would appear to be nearly zero in plots of the function. In the computer program the default value of μ is set equal to 100. This corresponds to taking $\Delta u = 0.135$ deg in Eq. (22). Taking a lower value of $\mu = 10$, to give more prominence to off-cusp values of G_{11}, corresponds to a value $\Delta u = 1.35$ deg.

3.3 Grid-Based Filtering of Short-Wavelength Noise

Figure 2 shows that the wavelengths change with θ and, in general, a wide range of wavelengths may be expected for an arbitrary $x - y$ grid of field points. Those waves where lengths are shorter than or comparable to the lengths Δx or Δy of the individual grid cell will show up as high frequency noise. In order to remove this noisy behavior in plots of the wave field, the program omits calculations for wavenumbers $\lambda_i (i = 1,2)$ which exceed the maximum wavenumber λ_M (minimum wavelength l_m) given by

$$\lambda_M = \frac{2\pi}{n \left[\min(\Delta x, \Delta y)\right]} \qquad (23)$$

where n is the number of grid points used to model the minimum wavelength. The default value is 4. A higher value of n may be used to focus on only the longer waves, while a lower value of n may be used to account for the shorter waves in spite of their possible noise-like appearance.

3.4 Description of Computer Program

Program RADGREEN consists of a main program and the subroutines CPTIME, FINROOT, FR1, and UNFORM. The main program accepts input data, performs various initializations, and carries out the calculations given in Eqs. (4)-(15) for a rectangular $x - y$ grid of field points. The CPTIME subroutine keeps track of the actual CPU time used for the calculations. As mentioned previously, the subroutines FINROOT and FR1 respectively perform global and local searches for the roots u of Eq. (8). The subroutine UNFORM writes onto an unformatted output file the calculated

8

value of the Green's function G_{11} (or the wave elevation z_s) and its slopes in a form suitable for three-dimensional and contour plots.

Input data are entered by means of an input file which conforms to the following READ statements.

```
        READ (5,521) filename
521   FORMAT (A30)
        READ (5,*) vel, gcal, nom, nsr, ipr, wnp, rmf, fmumx
        READ (5,*) (omga (m), m = 1, nom)
        READ (5,*) lcol, krow, x0, xdel, y0, ydel, eta, zeta
        DO 999 iom = 1, nom
        READ (5,*) (qamp (m), m = 1, nsr)
        READ (5,*) (qphd (m), m = 1, nsr)
        READ (5,*) (qxi(m), m = 1, nsr)
```

The input variables are defined as follows:

1. filename is the output file onto which are written the calculated values.

2. vel is the current or ship speed c in ft/s.

3. gcal is a calculation indicator such that for gcal ≥ 0.1, G_{11} is calculated; otherwise, z_s is calculated.

4. nom is the number of values of ω to be considered, $1 \leq$ nom ≤ 11.

5. nsr is the number of sources on the line $1 \leq$ nsr ≤ 21.

6. ipr is an output indicator such that for ipr ≥ 1 the calculated function (G_{11}) or z_s and its slopes are written onto the output file; otherwise, only the function itself is written.

7. wnp is n, defined in Eq. (23), the number of grid points used to model the minimum wavelength which will be considered in the calculations; entering wnp ≤ 0. triggers the default value wnp $= 4$.

8. rmf is the multiplier to establish R_{min} (the minimum value of R) to be used in Eq. (5) where $R_{min} =$ rmf * min $(\Delta x, \Delta y)$; if rmf is input $\leq 0.$, the default value rmf $= 10.$ is used.

9. fmumx is the maximum value of the magnification factor μ, defined in Eq. (19); entering fmumx $\leq 0.$ triggers the default value fmumx $= 100$.

10. omga (m) is the mth value of ω in rad/s, $1 \leq$ m $\leq$ nom.

11. lcol is the number of grid points in the x direction, $1 \leq$ lcol ≤ 151.

12. krow is the number of grid points in the y direction, $1 \leq$ krow ≤ 151.

13. x0 is the value of x in ft for the initial grid point.

14. xdel is the value of Δx in ft, the size of each grid cell in the x direction.

15. y0 is the value of y in ft for the initial grid point.

16. ydel is the value of Δy in ft, the size of each grid cell in the y direction.

17. eta is η in ft, the y value of the location of the line of sources.

18. zeta is ζ in ft, the z value of the location of the line of sources.

19., 20., 21. qamp (m), qphd (m), and qxi (m) are respectively the amplitude in ft^3/s, the phase in deg, and the x-location in ft of the mth source, $1 \leq m \leq nsr$; repeat for each new value of omga.

It should be emphasized that the singularity moderating factors rmf and fmumx, and the noise suppression factor wnp, have been implemented mainly to enhance the smoothness and visibility of overall plots of the calculated functional values. If such considerations are not of concern to the user, and the actual values of Eq. (5) are desired, then simply enter arbitrarily small nonzero values for rmf and wnp (such as 0.001) and a large value for fmumx (such as 9999).

Computer time at one field point for a single value of ω depends largely on the given value of τ. Using the Hewlett Packard 9000, Model 550 minicomputer, CPU time typically decreases from 0.3 seconds for $\tau \approx 0$ to 0.2 seconds for $\tau = 1$. Corresponding total CPU time for the maximum grid of 151 $\times$ 151 field points would vary between 115 and 75 minutes, approximately. Due to the approach used in Eq. (15), the calculation time for a line of sources differs little from that for a single source.

4. NUMERICAL RESULTS

A number of calculated results are presented to illustrate the capability of the program and the types of wave patterns to be expected from a single source and a line of sources for different values of the fundamental parameter $\tau = c\omega/g$. These results are presented in the form of three-dimensional and contour plots. Most of the results are presented in the form of the wave elevation z_s given by Eq. (13). Some results are also presented for the Green's function itself, Eq. (5), as well as the slopes defined by Eqs. (12) and (14).

By way of illustrating the symmetry properties about the x-axis, Figs. 3a, b, and c respectively sh sample plots of the wave elevation z_s, the x slope, and y slope for $\tau = 0.125$ for the square $-500 < x \leq 500$ and $-500 \leq y \leq 500$. These figures show that the calculated results con- the expected symmetry of z_s and its x slope, and the antisymmetry of the y slope about $y = 0$, which may be deduced from Eqs. (5), (13), and (14). Similar symmetry properties hold for the Green's function and its slopes.

In view of the above symmetry properties about $y = 0$, the remaining figures are shown only for one side of y, $0 \leq y \leq 450$ ft, and $-450 \leq x \leq 450$ ft, with $\Delta x = \Delta y = 6$ ft. The line of sources is taken to be submerged 6 ft ($\zeta = -6$) and with y coordinate $= 0$ ($\eta = 0$). Calculations are performed for a single source with x coordinate $= 0$ ($\xi = 0$) and for 10 equally spaced sources with $-135 \leq \xi \leq 135$ ft. This line may be taken to be the far field representation of a ship with draft 12 ft and length 300 ft. The strengths of the 10 sources are assumed to be either (a) equal or (b) linearly proportional to the ξ location of the source. Case (a) is an approximation to heave motions where the ship oscillates in the z direction, while case (b) is an approximation to pitch

10

motions where the ship undergoes rotational oscillations about the y axis. The angular frequency ω is fixed at 0.805 rad/s, which is representative of Sea State 5 conditions.

To show the difference between the wave elevation z_s and Green's function G_{11} cases, Figs. 4a, b, and c respectively show contour plots of z_s, $\partial z_s/\partial x$, and $\partial z_s/\partial y$ for $\tau = 0.125$, while Figs. 5a to c show corresponding plots for G_{11}. These figures show that the differences are relatively small.

Figures 6a to f show three-dimensional plots of z_s for the heave case for ship velocity $c = 0.2$, 5.0, 9.8, 10.2, 20.0, and 40.0 ft/s which correspond to $\tau = 0.005$, 0.125, 0.245, 0.255, 0.5, and 1.0. The highest speed may be considered representative of the design speed. These figures show how the wave pattern changes from ring waves to Kelvin type waves behind the ship as the velocity increases. Also, the previously mentioned cusp lines, which correspond to values of θ giving the vertical tangents in Fig. 2, appear for values of $\tau \geq 0.245$.

To illustrate the effect of source distribution on the wave pattern, Figs. 7a, b, c respectively show contour plots of z_s for $c = 0.2$ ($\tau = 0.005$) for the single source, heave, and pitch motions, while Figs. 8a to c show corresponding plots for $c = 9.8$ ($\tau = 0.245$). Figure 7a shows the expected symmetry about $x = 0$ of the ring waves from a single source at this near zero value of c. Relative to the nearly circular waves of the single source, Fig. 7b shows that the heave motion tends to concentrate the waves to the side of the ship (along the y axis) while the pitch motion tends to gives the largest waves fore and aft of the ship (along the x axis). In the case of the the more complex wave pattern for $c = 9.8$ ($\tau = 0.245$), the single source and pitch cases give similar wave patterns which are, in turn, more varied than those for the heave case.

5. SUMMARY

A previously formulated approach for calculating the far field behavior of the radiation Green's function G_{11}, corresponding to a source which is translating and oscillating beneath the free surface, has been numerically implemented in the form of computer program RADGREEN. Supplementary expressions have been derived for the far field derivatives of G_{11} as well as for the associated wave elevation and is derivatives. The program first uses a global scheme and then a localized scheme to determine the wave propagation directions u for a given spatial angle θ of the field point. It is shown that the behavior is regular at several apparent singular values of θ and u. However, at cusp lines which correspond to locations of vertical tangents in Fig. 2, the function does become unbounded and it is necessary to impose limits on the magnification of the waves at these points. It is also shown that the grid filtering technique removes short wavelength noise by retaining only those waves which have lengths equal to several cells of the computation grid. Calculation time on the HP 9000, Model 550 minicomputer for one field point varies from 0.3 seconds to 0.2 seconds, depending on the value of the dimensionless parameter $\tau = c\omega/g$.

A series of three-dimensional and contour plots are given to illustrate the capability of the program and to give representative wave patterns for a single source and for a ship undergoing heave and pitch motions. The heave and pitch motions are obtained by approximating the ship hull by a series of 10 sources on a line with source strengths which are respectively equal to each other and proportional to the longitudinal location of the source. These plots show that the program reproduces expected symmetry properties about the x and y axes. There is relatively little difference between contour plots of G_{11} and its derivatives and corresponding plots of z_s and its derivatives. At low speeds, relative to a single source, the wave pattern for heave motion tends to concentrate the waves to the side of the ship while the pitch motion produces the largest waves fore and aft of the ship.

6. ACKNOWLEDGMENT

7. REFERENCES

1. Liu, H.C., "Uber Die Entstehung von Ringwellen an einer Flüssigheitsoberfläche durch unter dieser gelegene, kugelige periodische Quellensysteme," *Zeitschrift für Angewandte Mathematik und Mechanik*, Vol. 32, pp. 221-226, July 1952.

2. Grekas, A. and Delhommeau, G., "Diffraction-radiation en présence d'un courant," *Bulletin de l'Association Technique Maritime et Aéronautique*, Vol. 83, pp. 293-319, 1983.

3. Eggers, K.W.H., Sharma, S.D., and Ward, L.W., "An Assessment of Some Experimental Methods for Determining the Wavemaking Characteristics of a Ship Form," *Transactions of the Society of Naval Architects and Marine Engineers*, Vol. 75, pp. 112-157, November 1967.

4. Newman, J.N., "Evaluation of the Wave-Resistance Green Function: Part 1 — The Double Integral," *Journal of Ship Research*, Vol. 31, No. 2, pp. 79-90, June 1987.

5. Wang, H.T. and Rogers, J.C.W., "Calculation of the Odd and Even Integral Components of the Wave Resistance Green's Function," NRL Memorandum Report 6411 (in press).

6. Chang, M.S., "Computation of Three-Dimensional Ship-Motions with Forward Speed," *The Proceedings of the Second International Conference on Numerical Ship Hydrodynamics*, pp. 124-135, September 1977.

7. Newman, J.N., "The Damping and Wave Resistance of a Pitching and Heaving Ship," *Journal of Ship Research*, Vol. 3, No. 2, June 1959.
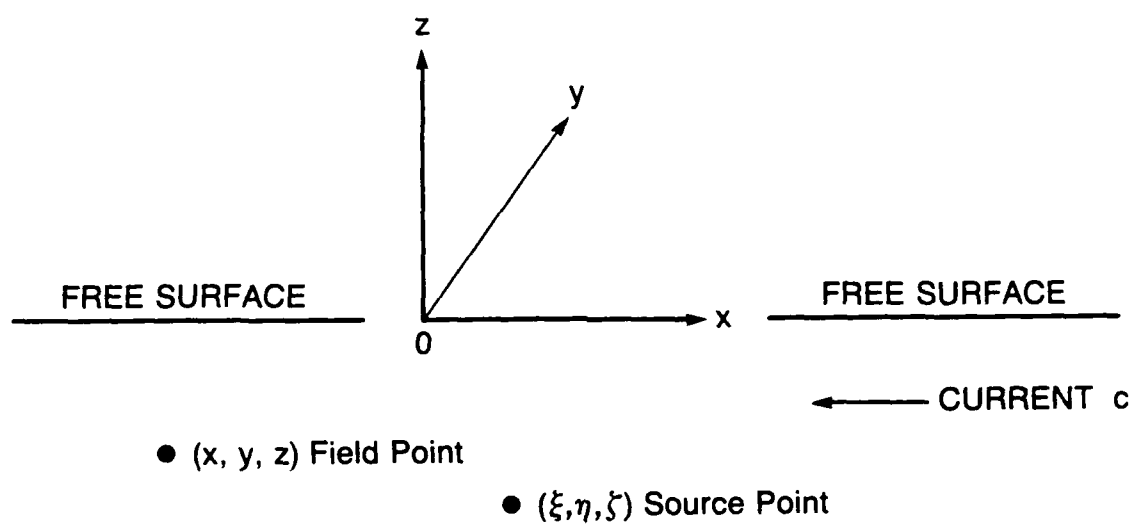
Fig. 1 — Definition of coordinate system
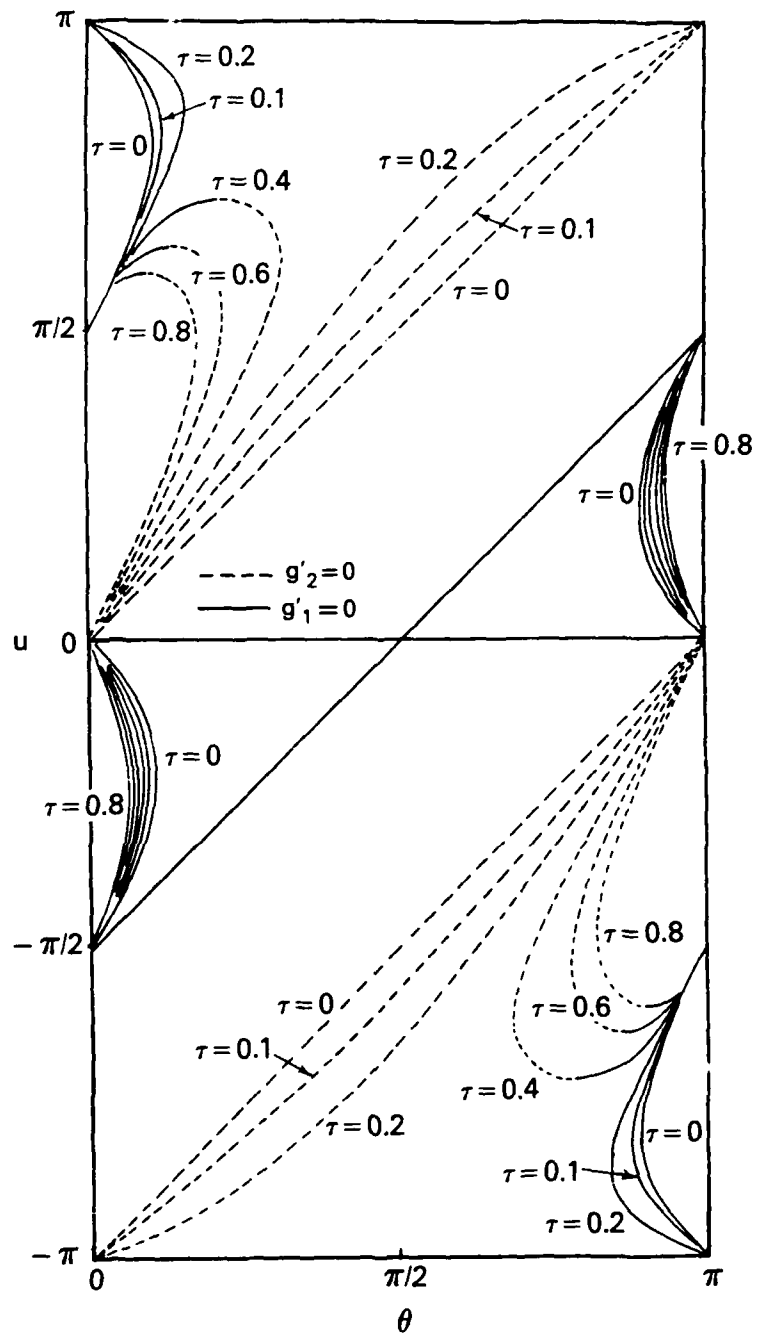
Fig. 2 — Curves representing the $u - \theta$ Equation (8) for various values of τ

14
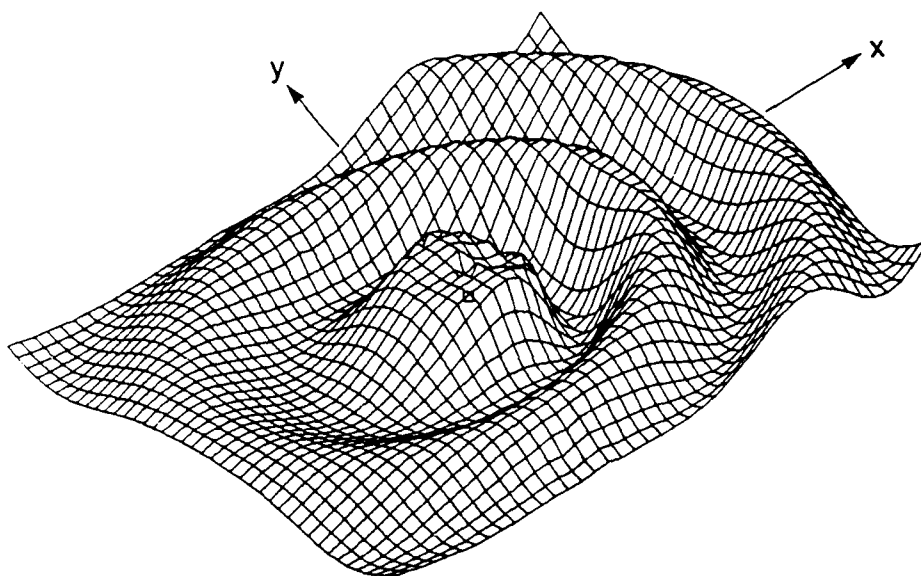
Fig. 3a — Elevation z_s
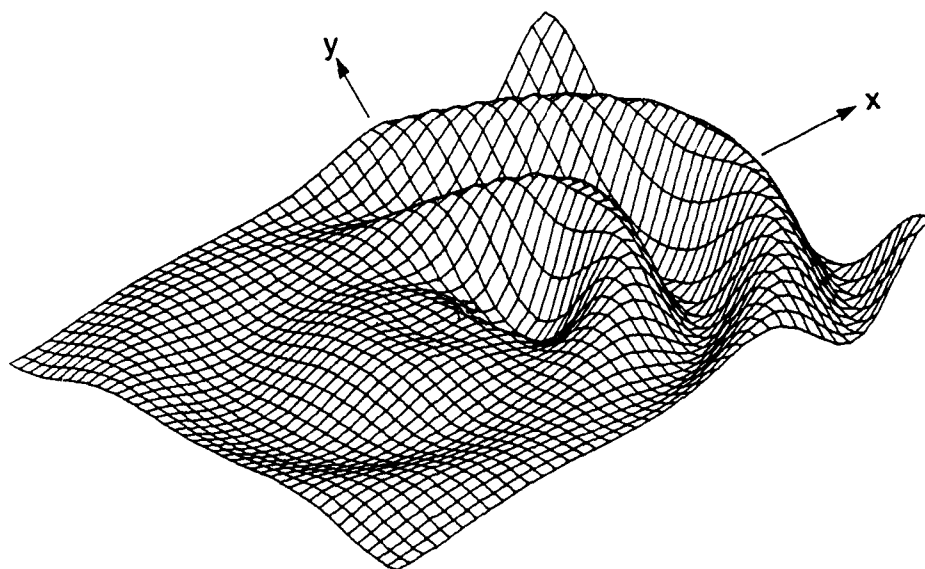
Fig. 3b — x-slope $\partial z_s / \partial x$

Fig. 3 — Sample three-dimensional plots of wave patterns, $\tau = 0.125$
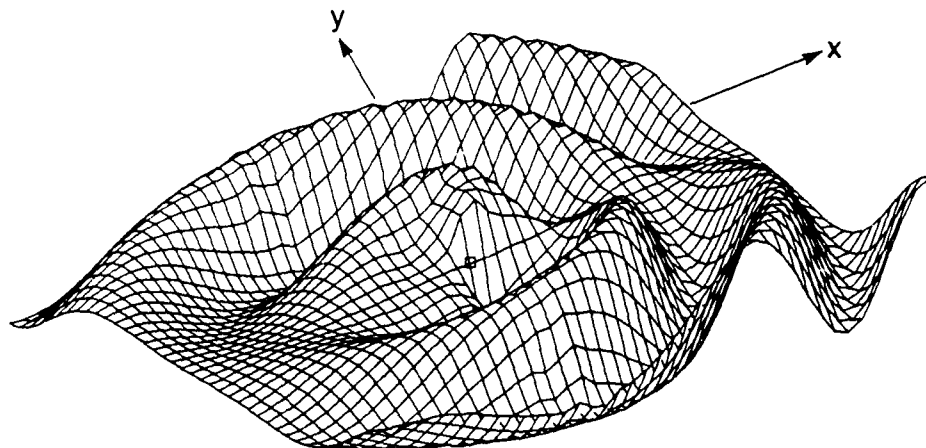
Fig. 3c — y-slope $\partial z_s / \partial y$

Fig. 3 — (Continued) Sample three-dimensional plots of wave patterns, $\tau = 0.125$
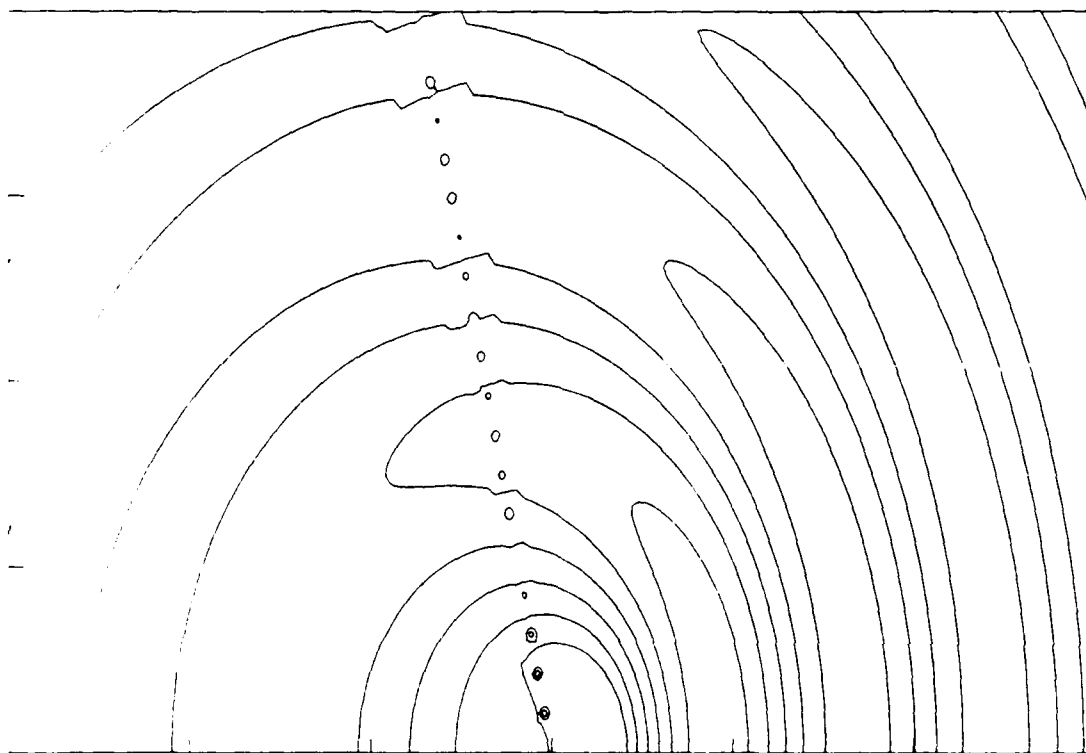
Fig. 4a — Elevation z_s

Fig. 4 — Contour plots of wave elevation z_s for single souce, $\tau = 0.125$
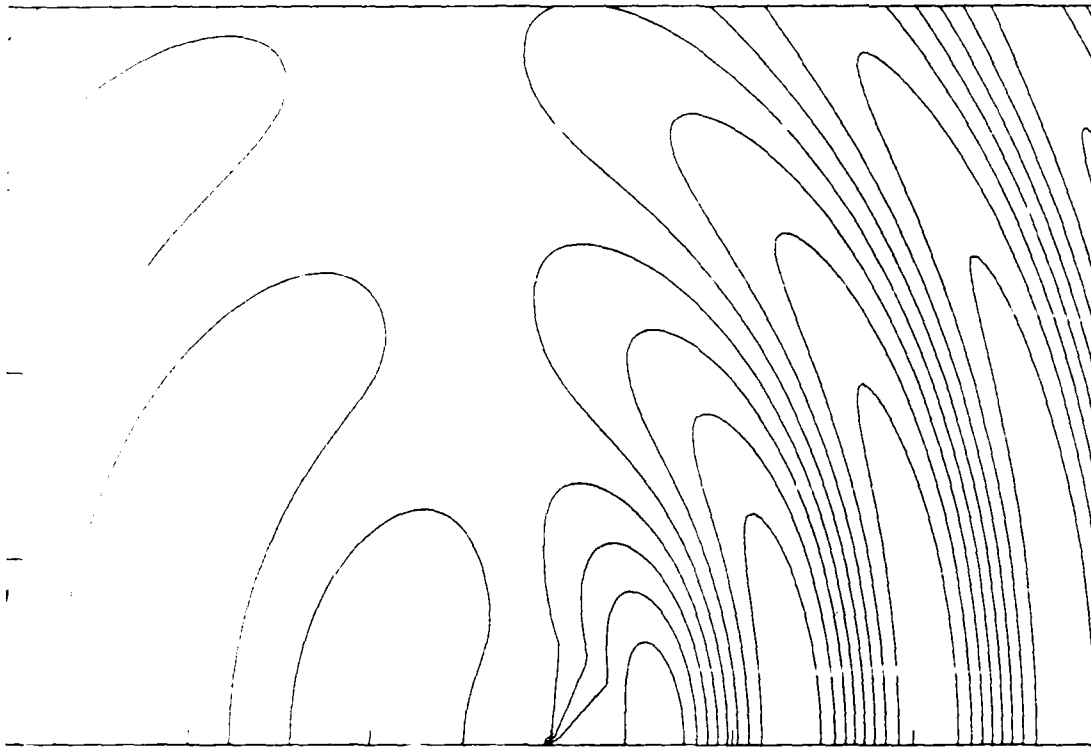
Fig. 4b — x-slope $\partial z_s / \partial x$
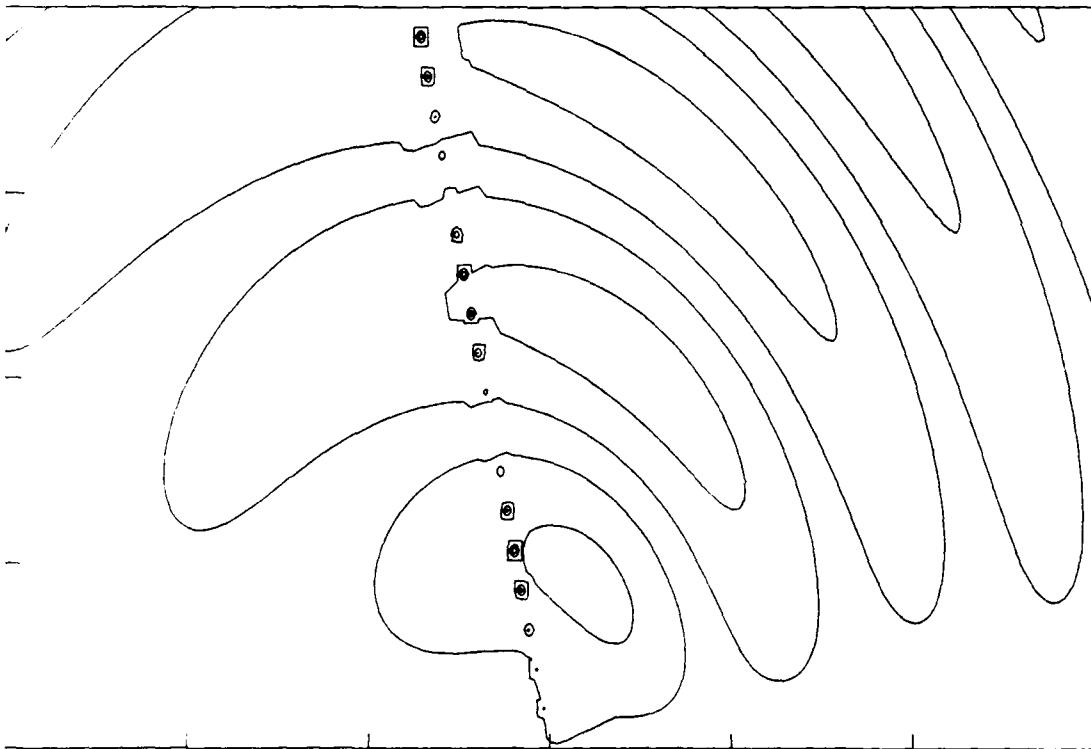
Fig. 4c — y-slope $\partial z_s / \partial y$

Fig. 4 — (Continued) Contour plots of wave elevation z_s for single souce, $\tau = 0.125$
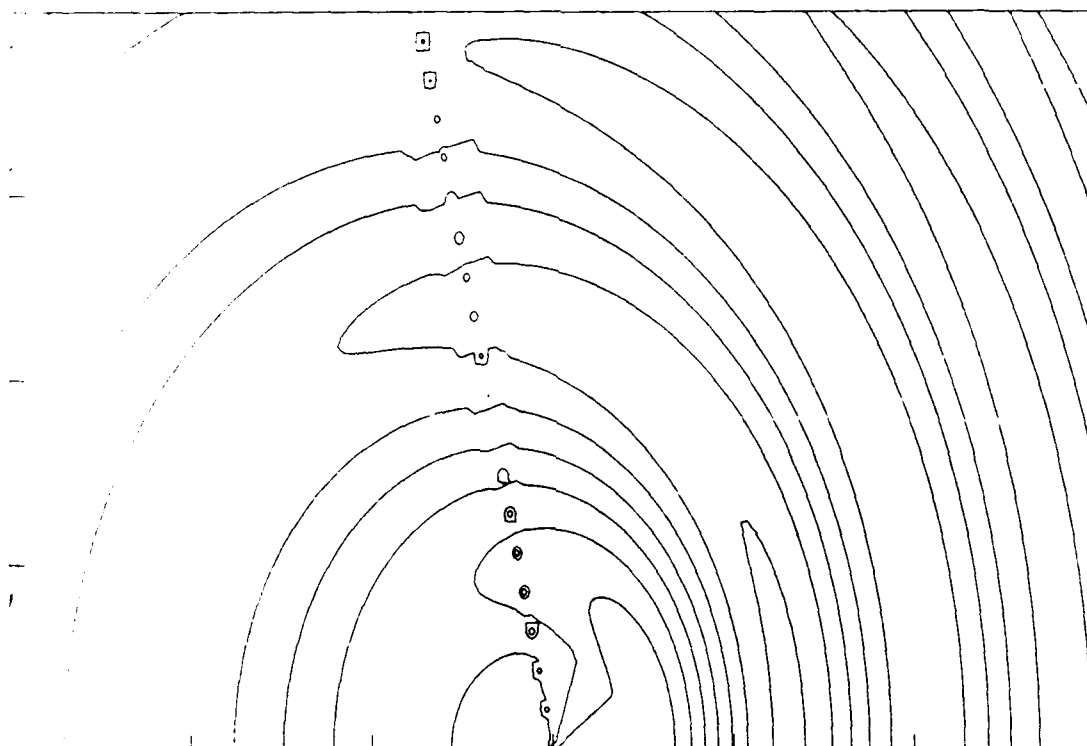
Fig. 5a — Green's function G_{11}
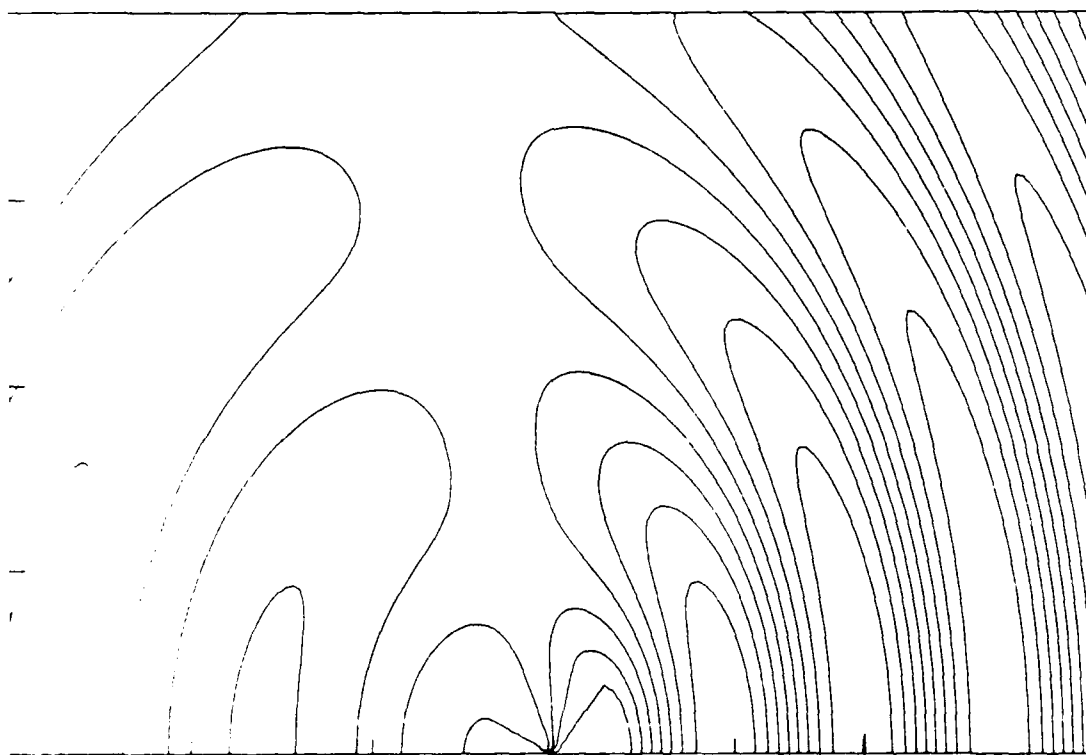
Fig. 5b — x-derivative $\partial G_{11}/\partial x$

Fig. 5 — Contour plots of Green's function G_{11} for single source, $\tau = 0.125$

18
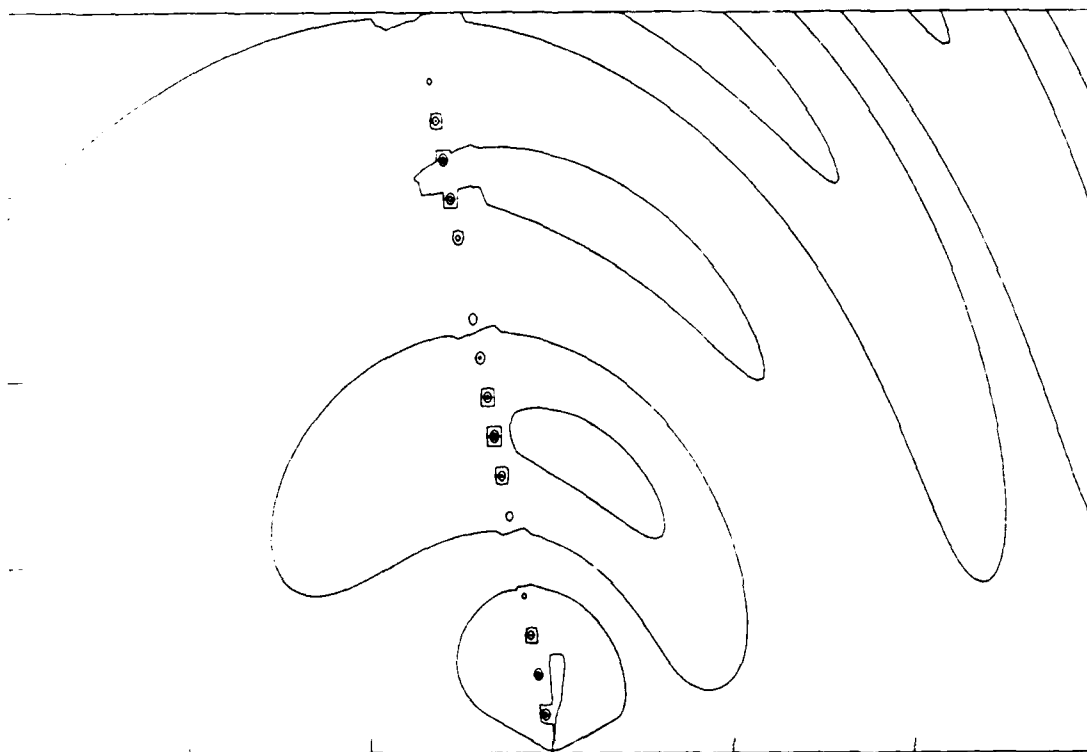
Fig. 5c — y-derivative $\partial G_{11}/\partial y$

Fig. 5 — (Continued) Contour plots of Green's function G_{11} for single source, $\tau = 0.125$
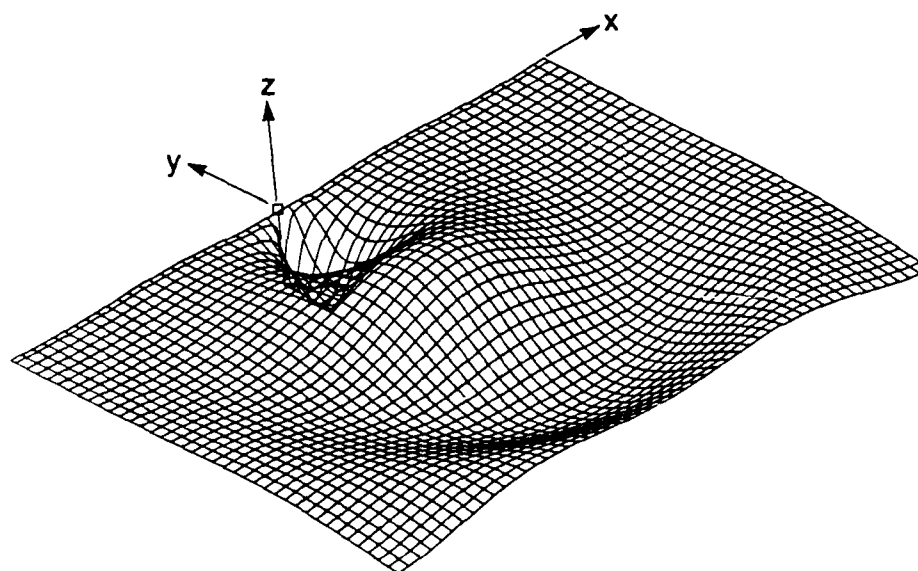
Fig. 6a — $c = 0.2$ ft/s, $\tau = 0.005$

Fig. 6 — Three-dimensional plots of heave wave elevation z_s
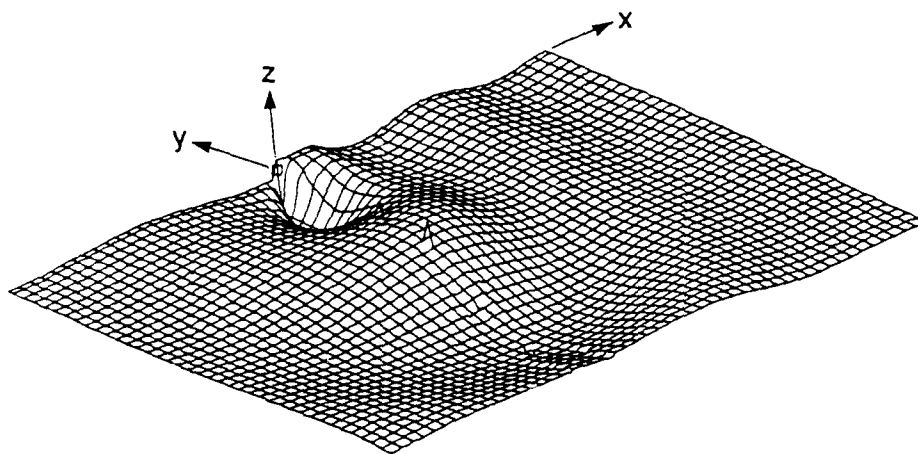
Fig. 6b — $c = 5.0$ ft/s, $\tau = 0.125$
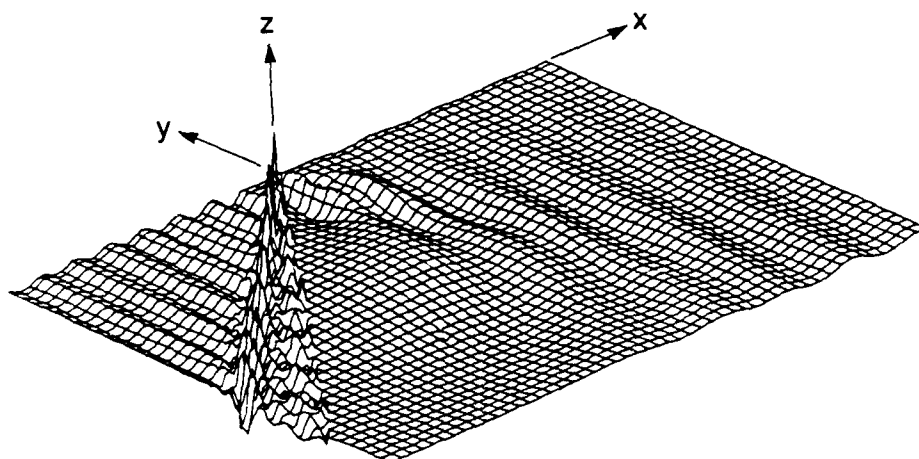
Fig. 6c — $c = 9.8$ ft/s, $\tau = 0.245$

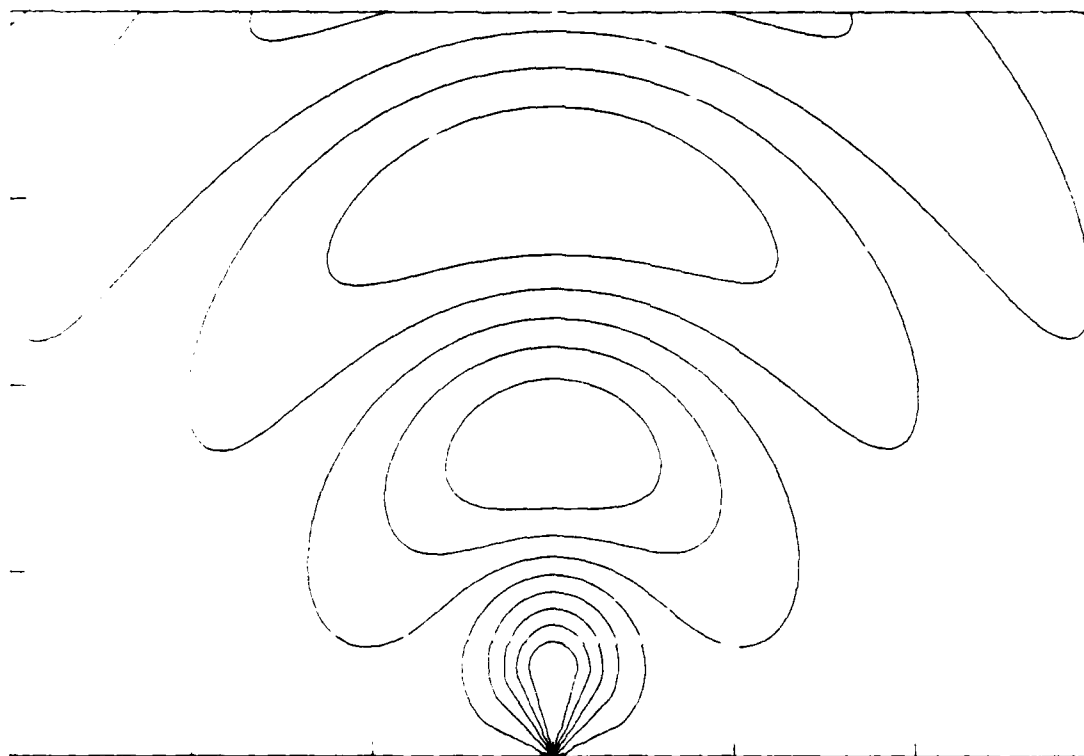Fig. 6 — (Continued) Three-dimensional plots of heave wave elevation z_s
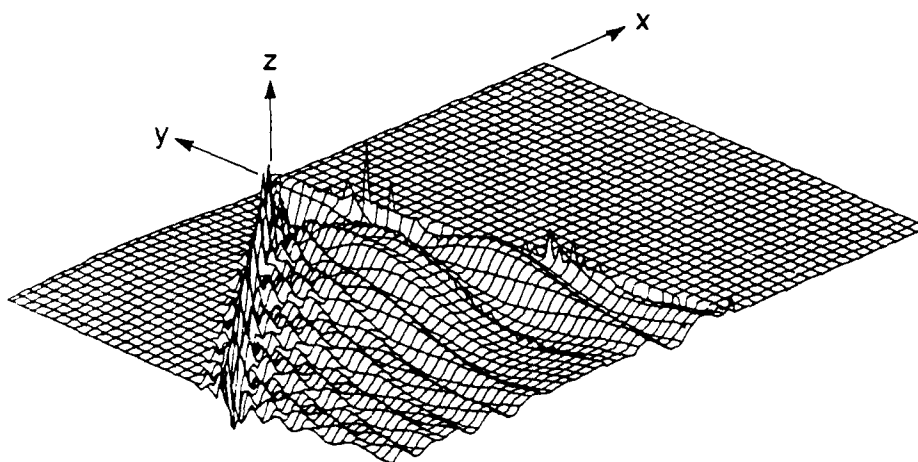
Fig. 6d — $c = 10.2$ ft/s, $\tau = 0.255$
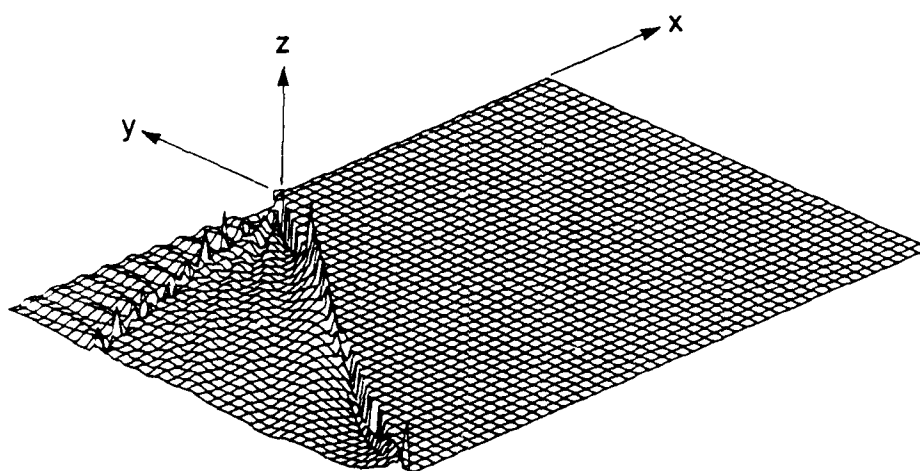
Fig. 6e — $c = 20.0$ ft/s, $\tau = 0.5$
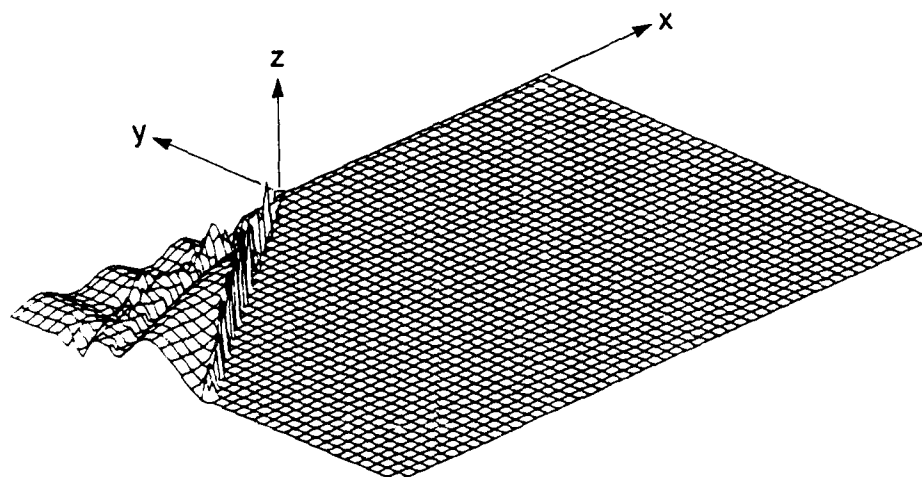
Fig. 6f — $c \approx 40.0$ ft/s, $\tau = 1.0$

Fig. 6 — (Continued) Three-dimensional plots of heave wave elevation z_s
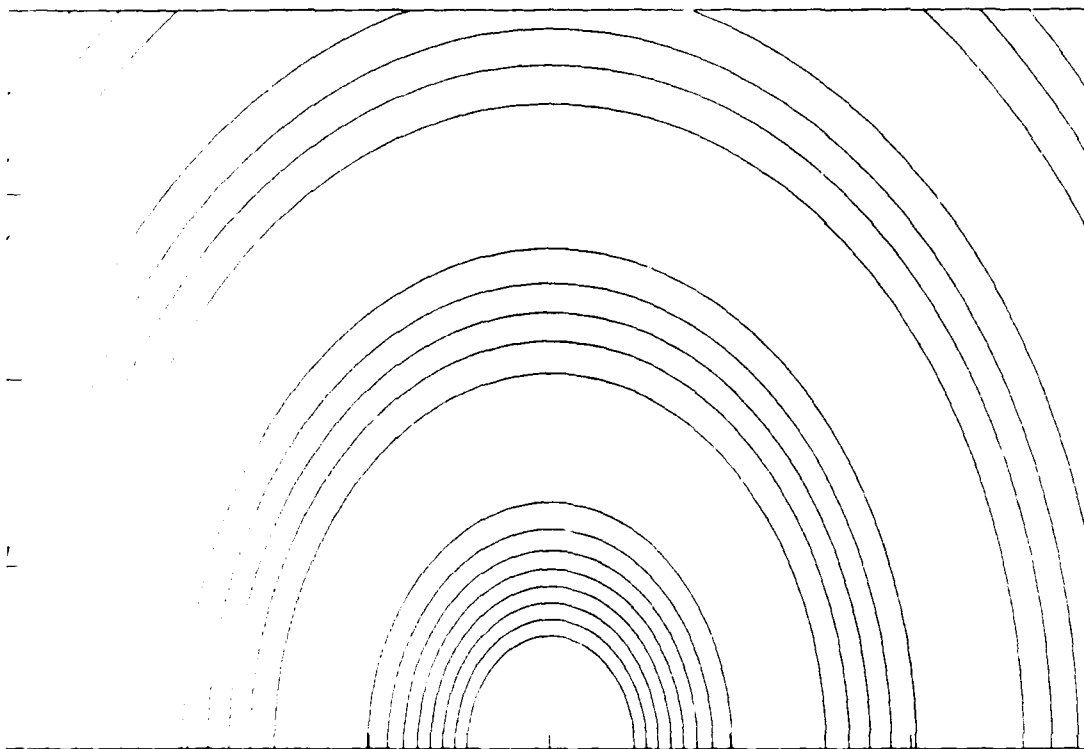
Fig. 7a — Single source

Fig. 7b — Heave for line of sources
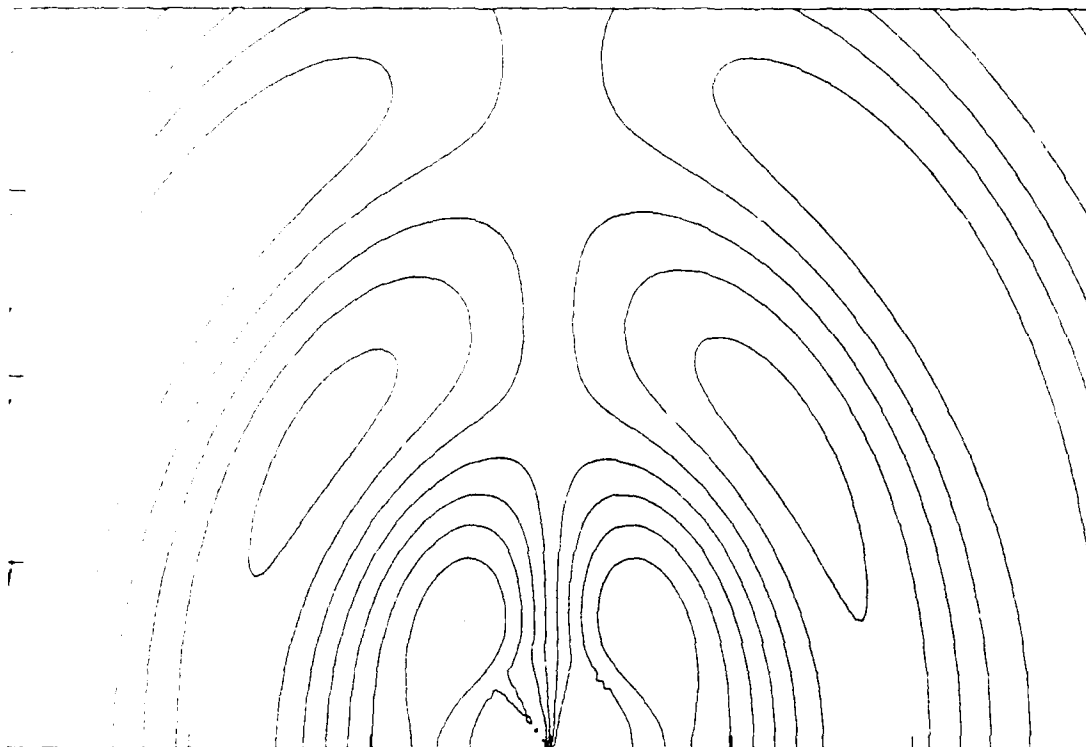
Fig. 7 — Contour plots of wave elevation z_s, $c = 0.2$ ft/s, $\tau = 0.005$

Fig. 7c — Pitch for line of sources

Fig. 7 — (Continued) Contour plots of wave elevation z_s, c = 0.2 ft/s, τ = 0.005
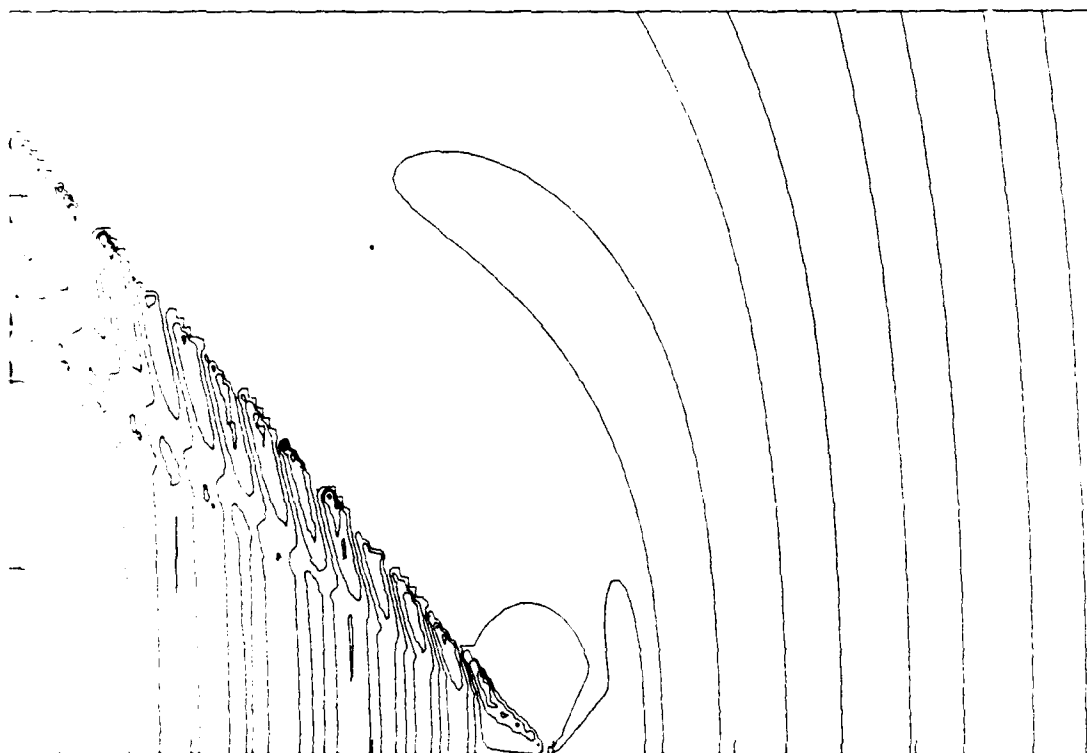

Fig. 8a — Single source

Fig. 8 — Contour plots of wave elevation z_s, c = 9.8 ft/s, τ = 0.245
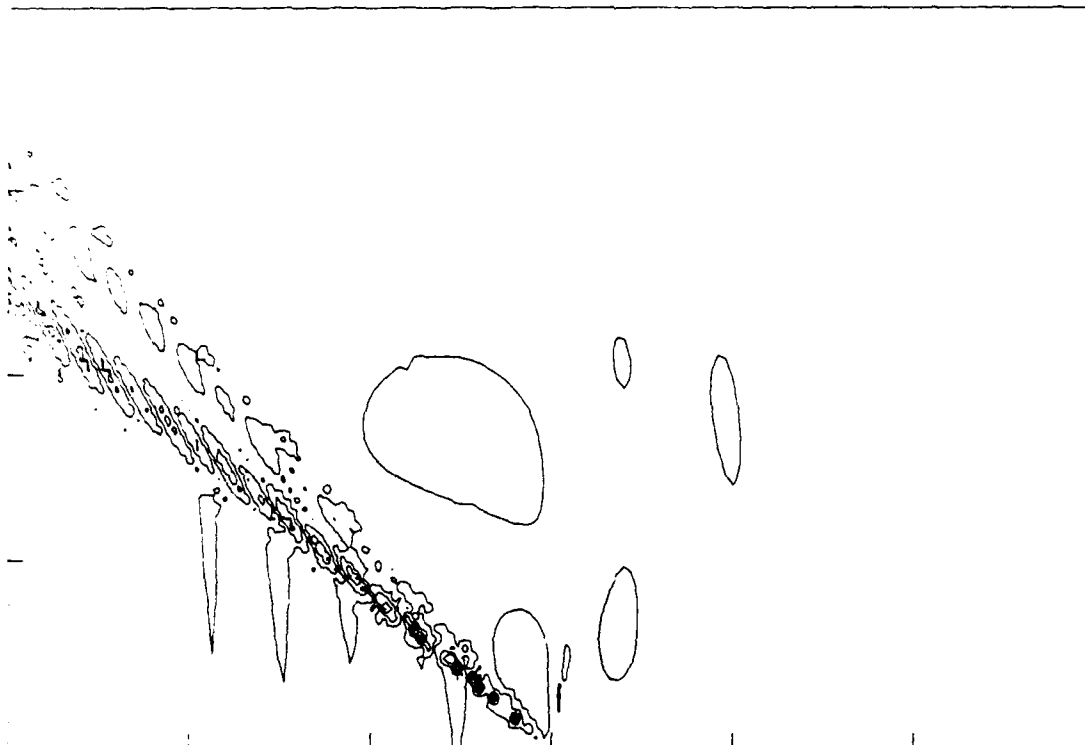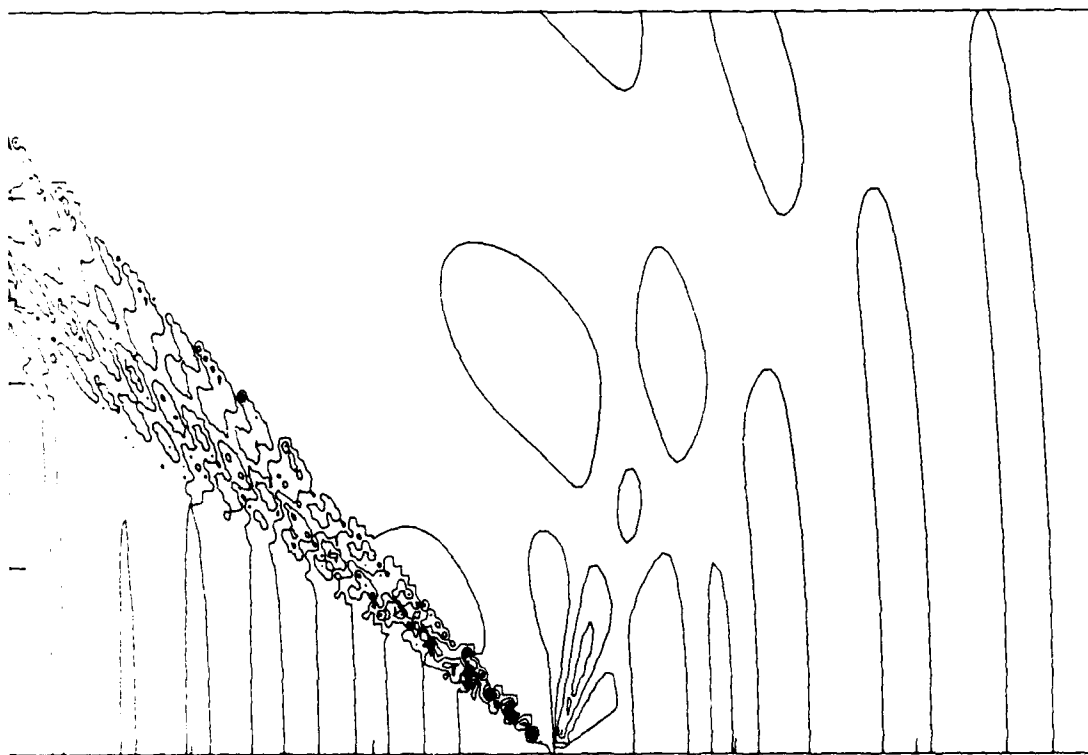
Fig. 8b — Heave for line of sources

Fig. 8c — Pitch for line of sources

Fig. 8 — (Continued) Contour plots of wave elevation z_s, $c = 9.8$ ft/s, $\tau = 0.245$